Peertechz

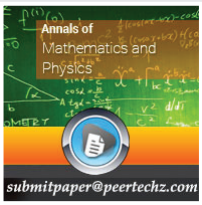

MATHEMATICS AND PHYSICS GROUP

ANNALS OF Mathematics and Physics OPEN ACCESS JOURNAL

ISSN: 2689-7636 DOI: https://dx.doi.org/10.17352/amp

Research Article

Linear Model of Vortex Ring

Tengfei Zheng[1,2]*, Wentao Wang[1,2] and Yuzong Yuan[1,2]

[1]School of Mechanical Engineering, Xi'an Jiaotong University, Xi'an, China

[2]State Key Laboratory for Manufacturing Systems Engineering, Xi'an Jiaotong University, Xi'an, China

Received: 28 October, 2025
Accepted: 05 November, 2025
Published: 06 November, 2025

***Corresponding author:** Tengfei Zheng, School of Mechanical Engineering, Xi'an Jiaotong University, Xi'an, China, E-mail: tengfz@xjtu.edu.cn

Keywords: Vortex ring; Linear mass-spring-damper system; Fluid-solid dynamics analogy; Linear modeling of vortex rings

https://www.mathematicsgroup.us

Check for updates

Abstract

Vortex rings represent canonical axisymmetric vortex structures in fluid mechanics, and understanding their dynamic behaviors is crucial for elucidating the generation, transport, and dissipation of vorticity. This paper introduces a novel vortex ring dynamics modeling method predicated on a linear mass-spring-damper system, thereby simplifying the vortex ring's motion to the dynamic response of a three-dimensional linear system. By discretizing the surrounding fluid into a finite number of particles and constructing a three-dimensional linear system to represent the encompassing flow field, the model accurately replicates vortex ring trajectories documented in established literature, achieving an average fitting error of less than 9%. The findings demonstrate that, with a damping coefficient of fv 0, the model effectively reproduces the closed trajectory characteristic of vortex rings in superfluids. Conversely, with $fv > 0$, it accurately captures the damped spiral motion observed in conventional fluids. This linear model circumvents the inherent complexities of traditional nonlinear approaches, offering an alternative analytical framework for investigating vortex ring dynamics, substantially reducing computational demands, and highlighting its potential for engineering applications in areas such as vortex ring control and fluid mechanical design.

Introduction

Vortex rings are fundamental structures in fluid mechanics, widely observed in industrial processes and natural environments. Investigating their generation and evolution is crucial for understanding fluid dynamics and advancing industrial applications. Since 1857, numerous scholars, including Helmholtz [1], Rankine [2], and Taylor [3], have extensively studied vortex rings in both classical fluids and superfluids [4], proposing various theoretical models to elucidate their formation and evolution. These models are primarily based on the Navier-Stokes (N-S) equations [5], with scholars developing nonlinear descriptions through the NS equations, which are then solved numerically. However, the inherent nonlinearity of fluid dynamics results in highly complex theoretical models and substantial computational costs, hindering precise prediction and control of large-scale vortex ring motion.

To study the global evolution of vortex rings, Kaden [6] simplified the vortex ring into a spiral curve. This approach, based on geometric feature analysis, significantly reduces computational complexity and improves efficiency. However, it does not fully account for dynamic processes of the fluid, limiting its applicability to qualitative explanations rather than broader fluid dynamics research.

However, our decomposition analysis reveals a new avenue for understanding vortex ring dynamics. Upon examining Kaden and other scholars' [7] simplified model, we observed that the two-dimensional (2D) vortex ring can be described as a damped oscillatory spiral. Further decomposition reveals that this 2D spiral can be split into two one-dimensional (1D) curves, both exhibiting damped oscillation characteristics. Drawing parallels between fluid dynamics and mechanical systems, we note that in control theory, complex systems are often simplified as linear mass-spring-damper systems. When subjected to an impulse input, the system's response manifests

Citation: Zheng T, Wang W, Yuan Y. Linear Model of Vortex Ring. Ann Math Phys. 2025;8(6):212-217. Available from: https://dx.doi.org/10.17352/amp.000166

as a 1D damped oscillatory curve. The similarity between these curves suggests that the underlying fluid behavior may be analogous to a linear mass-spring-damper system.

Based on this insight, we propose a novel linear vortex ring model, where the moving fluid is treated as a rigid body with finite mass, while the surrounding fluid is modeled as a three-dimensional (3D) linear mass-spring-damper system. To validate the model, we first employed 2D and 3D linear mass-spring-damper systems to fit experimentally obtained vortex ring trajectories from prior studies, as shown in Figure 1, achieving high fitting accuracy. Furthermore, in the zero-damping limit, such linear modeling successfully reproduced the characteristic motion of vortex rings in superfluids. The results demonstrate that our linear model effectively explains vortex ring generation mechanisms.

The analogy between fluid dynamics and linear mass-spring-damper systems introduces a novel paradigm to fluid mechanics. This approach significantly simplifies computational procedures while preserving accuracy, thereby establishing an innovative modeling framework for vortex ring dynamics research.

Modeling of vortex

Consider the classical one-dimensional linear second-order mass-spring-damping system, which comprises a mass block of mass (m), a spring with an elasticity coefficient k, and a damper with a damping coefficient f_v (Figure 2(a)). When a force $f(t)$ is applied to the mass block, it induces reciprocal motion in the x-direction, resulting in a displacement $x(t)$. The presence of damping causes the amplitude of this motion to gradually decrease, indicating that the mass block undergoes oscillatory motion with a decaying amplitude. The governing equation for this second-order system can be expressed as equation (1):

$$m\frac{d^2x(t)}{dt^2}+f_v\frac{dx(t)}{dt}+kx(t)=f_x(t) \quad (1)$$

If the input $f(t)$ is an impulse force, the displacement $x(t)$ of the mass block can be determined by equation (2):

$$x(t)=\frac{\omega_n e^{-\zeta\omega_n t}}{\sqrt{1-\xi^2}}*\sin(\omega_d t+\phi_1) \quad (2)$$

Where $\omega_n=\sqrt{\frac{k}{m}},\xi=\frac{f_v}{2\sqrt{mk}},\omega_d=\omega_n\sqrt{1-\xi^2}$.

The oscillatory motion path of a mass block subject to a unit impulse force can be determined by analyzing the system's dynamics. Consider a mass block with a weight of m $1kg$ and a spring with an elasticity coefficient of k $20N/m$. As illustrated in Figure 2(b), under undamped conditions (red curve, damping coefficient f_v = 0), the mass block exhibits vibrations of constant amplitude. In contrast, under damped conditions (blue curve, damping coefficient f_v = $0.6N.s/m$), the motion is characterized by oscillations that gradually decay over time. When comparing the trajectory of the mass block with that of a vortex ring, it becomes evident that the mass-spring damped system undergoes one-dimensional motion along a straight line, whereas the vortex ring moves within a two-dimensional plane with a diminishing radius. This observation leads to the hypothesis that a mass block constrained in a plane by a spring-damping system operating in two directions simultaneously would exhibit a trajectory akin to that of a vortex ring in a fluid. The conceptual setup of this system is depicted in Figure 3(a).

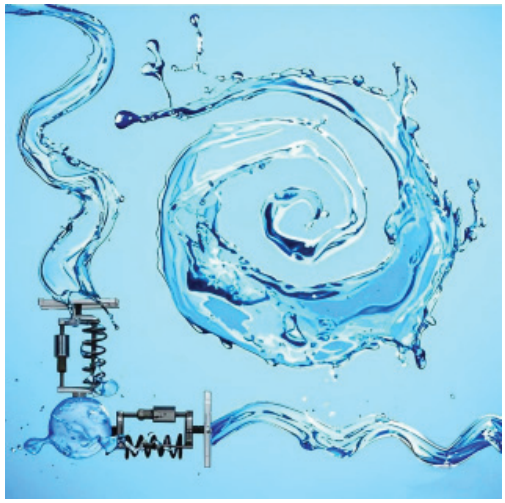

Figure 1: Schematic diagram of the model.

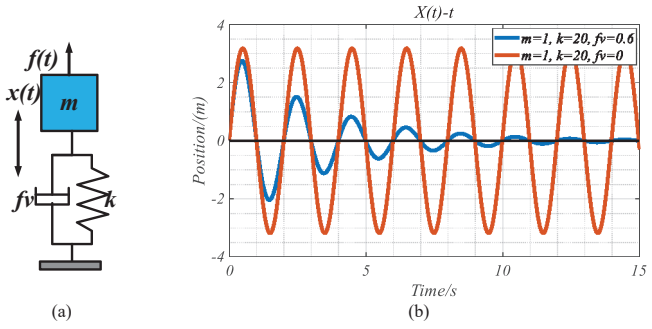

Figure 2: Schematic diagram of a one-dimensional mass-spring damping system and mass-block trajectory. (a) Schematic diagram of the mass-spring damping system (b) Displacement time curve of the mass block.

Assuming this, the control equation for the trajectory of mass block m is expressed as equation (3):

$$\begin{cases} m\frac{d^2x(t)}{dt^2}+f_{vx}\frac{dx(t)}{dt}+k_x x(t)=f_x(t) \\ m\frac{d^2y(t)}{dt^2}+f_{vy}\frac{dy(t)}{dt}+k_y y(t)=f_y(t) \end{cases} \quad (3)$$

Under the simplest computational conditions, with $f_x(t)$ and $f_y(t)$ as impulse forces, the displacement in both directions is given by Eq. (4):

$$\begin{cases} x(t)=\frac{\omega_n e^{-\zeta\omega_n t}}{\sqrt{1-\xi^2}}*\sin(\omega_d t+\phi_1) \\ y(t)=\frac{\omega_n e^{-\zeta\omega_n t}}{\sqrt{1-\xi^2}}*\sin(\omega_d t+\phi_2) \end{cases} \quad (4)$$

Where $\omega_n=\sqrt{\frac{k}{m}},\xi=\frac{f_v}{2\sqrt{mk}},\omega_d=\omega_n\sqrt{1-\xi^2}$。

Citation: Zheng T, Wang W, Yuan Y. Linear Model of Vortex Ring. Ann Math Phys. 2025;8(6):212-217. Available from: https://dx.doi.org/10.17352/amp.000166

Assuming a mass block with a weight of m = 1 kg and a spring elasticity coefficient of $k = 16\ N/m$ in both directions, the trajectory in a two-dimensional plane can be determined using the given formula, with phase angles $\Phi_1 = 0$ and $\Phi_2 = 0.3\pi$. As depicted in Figure 3(b), the trajectory of the undamped mass block forms an approximately elliptical closed curve, represented by the red curve, where the damping coefficients $f_{vx} = f_{vy} = o$. This trajectory bears resemblance to the vortex loop trajectory observed in superfluid dynamics. Conversely, when damping is introduced, with damping coefficients $f_{vx} = f_{vy} = 0.6\ N{\cdot}s/m$, the motion trajectory evolves into a spiral with a decreasing diameter, as shown by the blue curve in Figure 3(b). This behavior, characterized by oscillations that decay over time, aligns with the motion law of vortex ring trajectories in conventional fluids, thereby providing preliminary validation for our hypothesis.

To further validate the reliability of the theoretical model, we employed the model described by Eq. (3) to fit the vortex ring trajectories presented in PULLIN [7], specifically those depicted in Figure 4(a) and Figure 4(c), which serve as reference vortex ring curves. Notably, the vortex ring curves in Figure 4(a) exhibit unstable perturbations in the front section, resulting in data instability; thus, these data points were excluded from the fitting process. Given the uncertainty associated with the vortex ring size and the initial point of the vortex ring trajectory, it is hypothesized that a scaling factor applies to the vortex ring size, and the depicted trajectory represents a period following the generation of the vortex ring. Consequently, scaling coefficients k_x, k_y, along with the leading time term t_o, are introduced into the vortex ring trajectory fitting. At this juncture, the second-order linear model of the vortex ring is reformulated from Eq. (4) into the format of Eq. (5):

$$\begin{cases} x(t) = k_x * \dfrac{\omega_n e^{-\zeta\omega_n(t_0+t)}}{\sqrt{1-\xi^2}} * \sin(\omega_d t + \phi_1) \\ y(t) = k_y * \dfrac{\omega_n e^{-\zeta\omega_n(t_0+t)}}{\sqrt{1-\xi^2}} * \sin(\omega_d t + \phi_2) \end{cases} \tag{5}$$

The phase angles Φ_1 and Φ_2 are calculated according to equation (6):

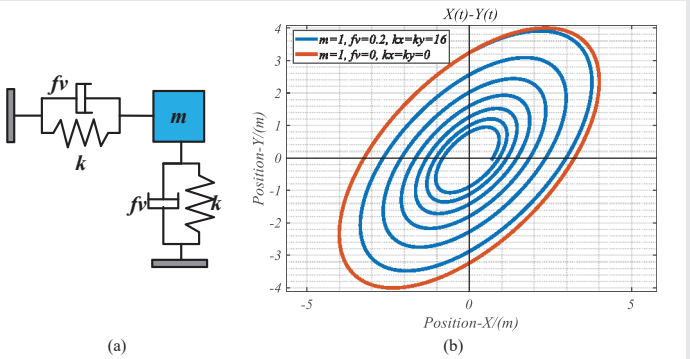

Figure 3: Schematic diagram of the 2D mass-spring damping system and mass-block trajectory. (a)Schematic diagram of a two-dimensional mass-spring damping system (b) Displacement time curve of a mass block.

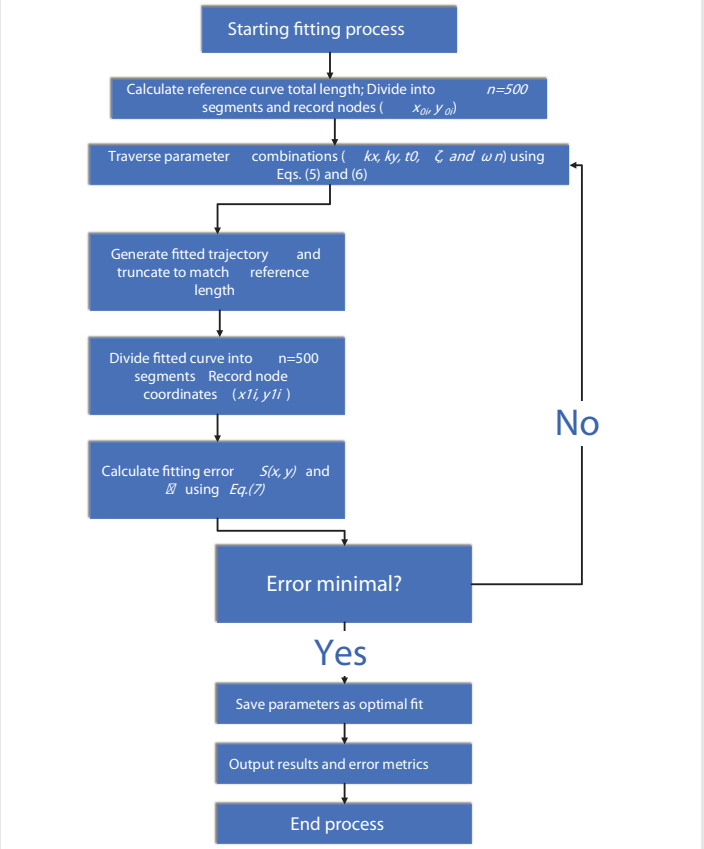

Figure 4: Flowchart of vortex ring fitting process.

$$\begin{cases} x(0) = k_x * \dfrac{\omega_n e^{-\zeta\omega_n(t_0)}}{\sqrt{1-\xi^2}} * \sin(\phi_1) \\ y(0) = k_y * \dfrac{\omega_n e^{-\zeta\omega_n(t_0)}}{\sqrt{1-\xi^2}} * \sin(\phi_2) \end{cases} \tag{6}$$

According to Eq. (6), it has been established that the fitted curve initiates concurrently with the target curve, and the vortex ring trajectory is modeled using MATLAB. The fitting procedure is detailed as follows:

The total length of the reference vortex loop curve is calculated through integration, and this length is divided into $n = 500$ equal segments. The node coordinates (x_{oi}, y_{oi}) for each sub-segment are recorded;

Utilizing Eq. (5) and Eq. (6), the fitted vortex ring trajectories are generated using the ergodic method under various combinations of parameters k_x, k_y, t_o, ζ, and ω_n;

The length of the fitted vortex loop trajectory is truncated to match the length of the reference vortex loop curve. This truncated section is then divided into $n = 500$ equal segments, and the node coordinates (x_{1i}, y_{1i}) for each segment are documented.

The fitting errors between the fitted vortex ring curves and the reference vortex ring curves are compared. The set of fitted parameters that yields the smallest fitting error is considered the optimal fitting result.

Citation: Zheng T, Wang W, Yuan Y. Linear Model of Vortex Ring. Ann Math Phys. 2025;8(6):212-217. Available from: https://dx.doi.org/10.17352/amp.000166

We have also prepared a flowchart, as shown in Figure 4.

Given the complexity of the vortex loop curve and the non-uniformity of *x*-coordinates and *y*-coordinates between the reference curve and the fitted curve, traditional error calculation methods, such as the least squares method and the goodness-of-fit, are not applicable. Instead, the fitting error is computed by evaluating the difference in the average distance of the *xy*-coordinates between corresponding nodes of each segment of equal length. This trajectory fitting error, $S(x, y)$, and the percentage of error, Δ, are calculated as shown in Eq. (7).

$$S(x,y)=\frac{\sum_{i=1}^{n}\left|(x_{0i}-x_{1i})^2+(y_{0i}-y_{1i})^2\right|}{2n}$$
$$\Delta=\frac{S(x,y)}{(\sum_{i=1}^{n}|x_{0i}|+\sum_{i=1}^{n}|y_{0i}|)/(2n)}\times 100\% \quad (7)$$

The optimal fitting trajectory of the vortex ring, determined by the smallest $S(x,y)$ and the smallest Δ, is depicted in Figure 5(b) and Figure 5(d), representing the best fitting result of the vortex ring trajectory using the specified calculation method. In Figure 5(b), the fitting results correspond to the vortex ring trajectory shown in Figure 5(a), with fitting parameters k_x = *0.200*, k_y = *0.260*, t_o = *0.850s*, ζ = *0.042N.s/m*, and ωn = *0.610rad/s*. The average distance difference of the *xy*-coordinates for each segmented node is *0.0054m*, resulting in an error percentage of Δ = *8.96%*. Similarly, Figure 5(d) illustrates the fitting results for the vortex ring trajectory depicted in Figure 5(c), with fitting parameters k_x = *0.390*, k_y = *0.390*, t_o = *0.120s*, ζ = *0.040N.s/m*, and ω_n = *0.490rad/s*. Here, the average distance difference in the *xy*-coordinates for each segment node is *0.0064m*, with an error percentage of Δ = *7.67%*.

The high degree of similarity and closeness between the fitted vortex ring curves and the reference curves, along with the minimal fitting distance error between corresponding segmented points, effectively demonstrates the validity and accuracy of the theoretical model proposed in this paper.

Following the fitting of the vortex ring trajectory, an analysis of the vortex ring's velocity characteristics is performed using this model. Specifically, the linear velocity components (v_x, v_y), the resultant velocity (v_r), and the angular velocity (ω) of the vortex ring can be derived from Eq. (5) and are expressed in Eq. (8). Based on the established fitting model and Eq. (8), the velocity distributions of these components along the vortex ring trajectories, specifically for the cases shown in Figure 4(b) and Figure 4(d), are presented in Figure 6.

$$\begin{cases} v_x=\dfrac{dx(t)}{dt} \\ v_y=\dfrac{dy(t)}{dt} \\ v_r=\sqrt{v_x^{\,2}+v_y^{\,2}} \\ \omega=\dfrac{x(t).v_y-y(t).v_x}{\sqrt{v_x^{\,2}+v_y^{\,2}}} \end{cases} \quad (8)$$

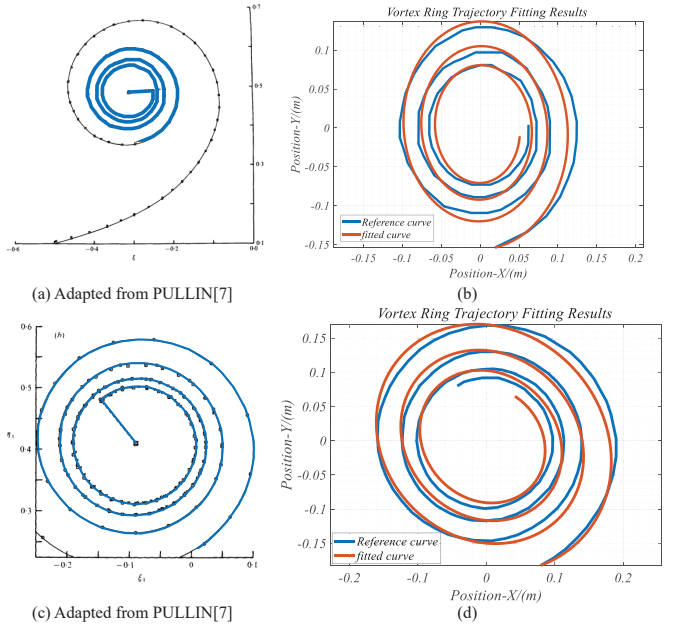

Figure 5: Second-order linear model fitting results for vortex loop paths. (a) Vortex loop trajectory1 of PULLIN[7] (blue curve is the fitted segment) (b) Fitting results to the vortex loop trajectory of Figure 3(a). (c) Vortex loop trajectory2 of PULLIN[7] (blue curve is the fitted segment) (d) Fitting results to the vortex loop trajectory of Figure 3(c).

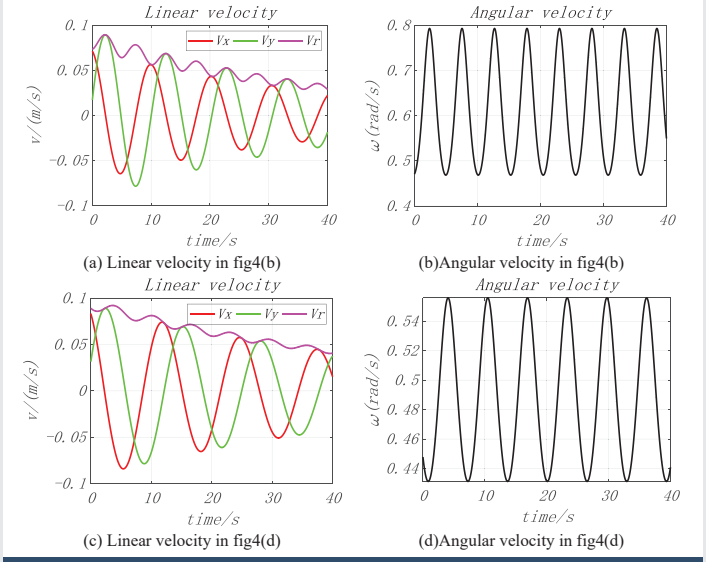

Figure 6: Velocity results of vortex rings in Figure 5.

As depicted in Figure 6, the linear velocity (v_x, v_y & v_r) of the vortex ring exhibits an oscillating and decaying trend. The gradual decrease in the vortex ring radius is consistent with the dissipative effects of fluid resistance acting on it. Conversely, the angular velocity ω of the vortex ring maintains a stable oscillatory process, with its amplitude appearing unaffected by the vortex ring's changing radius. This stability in angular velocity is fundamentally linked to the conserved or quasi-conserved nature of the vortex ring's circulation [8]. Consequently, the amplitude of the angular velocity does not decay, which highlights the ability of the proposed theoretical model to accurately describe this aspect of the vortex ring's velocity characteristics [9,10].

Citation: Zheng T, Wang W, Yuan Y. Linear Model of Vortex Ring. Ann Math Phys. 2025;8(6):212-217. Available from: https://dx.doi.org/10.17352/amp.000166

In the previous analysis, we developed a two-dimensional vortex ring second-order linear model, Eq. (3), by considering the system input force *f(t)* as an impulse force. To extend this model to a three-dimensional vortex ring, the model equations are presented in Eq. (9):

$$\begin{cases} m\dfrac{d^2x(t)}{dt^2} + f_{vx}\dfrac{dx(t)}{dt} + k_x x(t) = f_x(t) \\ m\dfrac{d^2y(t)}{dt^2} + f_{vy}\dfrac{dy(t)}{dt} + k_y y(t) = f_y(t) \\ m\dfrac{d^2z(t)}{dt^2} + f_{vz}\dfrac{dz(t)}{dt} + k_z z(t) = f_z(t) \end{cases} \quad (9)$$

The second-order linear model for a 3D vortex ring, based on Equation (9), is applied to the vortex ring trajectories described in the works of Chevalier [11] (Figure 7(a)) and Scheeler [12] (Figure 8(a)). Due to the absence of specific coordinate data in these papers, the trajectories are fitted based on similar features. In the analysis of the vortex ring trajectory depicted in Figure 7(a), an attenuated vortex ring curve is observed in the *yz* plane, with the trajectory progressing along the *x*-axis. Reflecting these characteristics, the parameters for the yz direction are set as $\omega_n = 2$ and $\zeta = 0.2$, while the excitation described in Equation (10) is applied in the *x* direction. By substituting into the model of Equation (9), the vortex ring trajectory is fitted, resulting in the fitting equation provided in Equation (11). The fitting outcome, illustrated in Figure 7(b), demonstrates a curve with trajectory characteristics closely resembling those of the vortex ring curve in Figure 7(a).

$$\begin{cases} f_z(t) = 0.5kt + 0.5c + 0.1(k - m\omega_d)\sin(\omega_d t) + 0.1c\omega_d \cos(t) \\ \omega_d = \omega_n\sqrt{1-\xi^2} \end{cases} \quad (10)$$

$$\begin{cases} x(t) = \dfrac{2e^{-\xi\omega_n t}}{\sqrt{1-\xi^2}}\sin(2\sqrt{1-\xi^2}\,t) \\ y(t) = \dfrac{2e^{-\xi\omega_n t}}{\sqrt{1-\xi^2}}\sin(2\sqrt{1-\xi^2}\,t + 0.5\pi) \\ z(t) = 0.5t + 0.01\sin(2\sqrt{1-\xi^2}\,t) \end{cases} \quad (11)$$

Figure 8(a) illustrates the trajectory of a vortex ring in a superfluid, characterized by a closed curve in the *xy*-plane and exhibiting periodic sinusoidal fluctuations along the *z*-axis. To capture the dynamics of this vortex ring trajectory, the excitation force described in Equation (12) is employed. By substituting the model from Equation (9), we derive a fitting equation, presented as Equation (13), that aligns with the vortex ring trajectory. The results of this fitting process are depicted in Figure 8(b), where the fitted curves demonstrate trajectory characteristics similar to those of the vortex ring curves shown in Figure 8(a).

$$\begin{cases} f_x(t) = (2k - 8m)\sin(2t) + 4c\cos(2t) \\ f_y(t) = (2k - 8m)\sin(2t) - 4c\cos(2t) \\ f_z(t) = (0.1k - 40m)\sin(20t) + 2c\cos(20t) \end{cases} \quad (12)$$

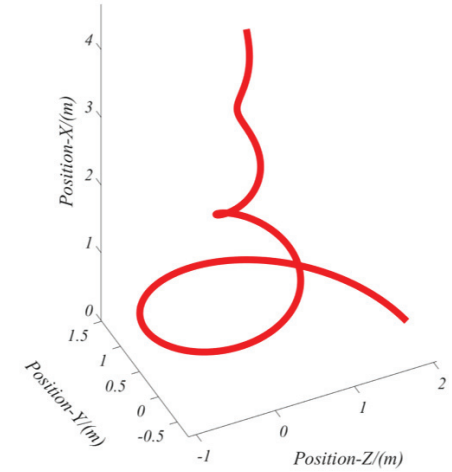

Figure 7: Three-dimensional vortex ring fitting results with vortex ring trajectory of Chevalier [11].

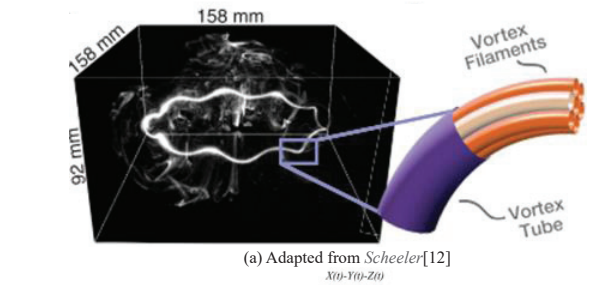

(a) Adapted from *Scheeler*[12]

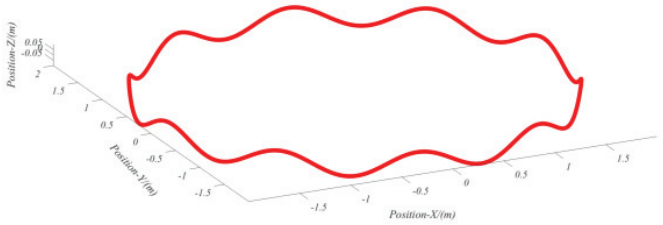

(b)

Figure 8: Three-dimensional vortex ring fitting results (a) Vortex ring trajectory of *Scheeler* [12] (b) Fitting results to the vortex ring trajectory of Figure (6a).

$$\begin{cases} x(t) = 2\sin(2t) \\ y(t) = 2\sin(2t + 0.5\pi) \\ z(t) = 0.1\sin(20t) \end{cases} \quad (13)$$

This underscores the validity and precision of the second-order linear model of vortex rings proposed in this study, suitable for fitting 2D and describing 3D vortex ring trajectories.

Summary

This study introduced a vortex ring linear theory model predicated on a linear mass-spring-damper system. The model effectively characterized the kinematic behavior of two-dimensional vortex rings and was subsequently extended to successfully describe the trajectory characteristics of three-dimensional vortex rings. These findings suggest that a vortex ring model based on a linear mass-spring system can effectively represent the physical behavior of vortex fluids in three-dimensional space. Notably, this model applies to both

Citation: Zheng T, Wang W, Yuan Y. Linear Model of Vortex Ring. Ann Math Phys. 2025;8(6):212-217. Available from: https://dx.doi.org/10.17352/amp.000166

conventional fluid vortex rings and undamped superfluid vortex rings. This approach significantly simplifies the mathematical modeling of vortex ring characteristics in fluids, thereby broadening the methodological approaches within vortex ring theory and offering substantial value for engineering applications related to fluid properties.

Acknowledgment

This work was supported by the Advanced Jet Propulsion Innovation Center, AEAC(Project ID.HKCX2024-01-030).

References

1. Helmholtz H. Über Integrale der hydrodynamischen Gleichungen, welche den Wirbelbewegungen entsprechen. J Reine Angew Math. 1858;55:25–55. Available from: https://www.scirp.org/reference/referencespapers?referenceid=1989127

2. Rankine WJM. A Manual of the Steam Engine and Other Prime Movers. Rev. by Millar WJ. London: Griffin; 1858. Available from: https://archive.org/details/amanualsteameng03rankgoog

3. Taylor GI. Experiments on the motion of solid bodies in rotating fluids. Proc R Soc Lond A. 1923;104:213–8. Available from: https://doi.org/10.1098/rspa.1923.0103

4. Kaden H. Unwinding of an unstable discontinuity surface. Ing Arch. 1931;2:140–68.

5. Harlow FH, Welch JE. Numerical calculation of time-dependent viscous incompressible flow of fluid with free surface. Phys Fluids. 1965;8:2182–9. Available from: https://doi.org/10.1063/1.1761178

6. Smith JHB. Improved calculations of leading-edge separation from slender, thin, delta wings. Proc R Soc Lond A. 1968;306:67–90. Available from: https://royalsocietypublishing.org/doi/10.1098/rspa.1968.0138

7. Pullin DI. The large-scale structure of unsteady self-similar rolled-up vortex sheets. J Fluid Mech. 1978;88:401–30. Available from: https://doi.org/10.1017/S0022112078002189

8. Didden N. On the formation of vortex rings: rolling-up and production of circulation. Z Angew Math Phys. 1979;30:101–16. Available from: https://ui.adsabs.harvard.edu/link_gateway/1979ZaMP...30..101D/doi:10.1007/BF01597484

9. Salomaa MM, Volovik GE. Quantized vortices in superfluid He3. Rev Mod Phys. 1987;59:533–613. Available from: https://journals.aps.org/rmp/abstract/10.1103/RevModPhys.59.533

10. Zheng T, Liu X, Wang C, Liu Z. Second-order linear model of vortex street. 2023. Available from: https://www.researchgate.net/publication/372492270_Second-order_linear_model_of_Karman_vortex_vortex

11. Chevalier Q, Douglas CM, Lesshafft L. Resolvent analysis of swirling turbulent jets. Theor Comput Fluid Dyn. 2024;38:641–63. Available from: https://dspace.mit.edu/handle/1721.1/159016

12. Scheeler MW, Van Rees WM, Kedia H, Kleckner D, Irvine WTM. Complete measurement of helicity and its dynamics in vortex tubes. Science. 2017;357:487–91. Available from: https://doi.org/10.1126/science.aam6897

Citation: Zheng T, Wang W, Yuan Y. Linear Model of Vortex Ring. Ann Math Phys. 2025;8(6):212-217. Available from: https://dx.doi.org/10.17352/amp.000166